DESIGN, DIMENSIONING AND AUTOMATED MANUFACTURING OF PROFILED COMPOSITE DRIVESHAFTS

W. Hufenbach[1], F. Lenz[1*], M. Birke[1], S. Spitzer[1], S. Münter[1]
[1]Institute of Lightweight Design and Polymer Technologies, Technische Universität Dresden, Dresden, Germany
* Corresponding author (florian.lenz@tu-dresden.de)

Keywords: *driveshaft, composite material, load introduction, continuous manufacturing, spline joint*

1 Introduction

International competition and political guidelines regarding a significant reduction in greenhouse gas emission demand a higher efficiency in machine manufacturing and operation [1, 2]. Especially in the field of mobility systems, lightweight designs utilizing carbon fiber reinforced plastics (CFRP) are used more and more to lower the mass and energy consumption of airplanes, automobiles and ships Aside the outstanding mechanical performance of CFRPs, functional benefits like corrosion resistance and high internal damping coefficients can also substantiate the use of those high tech materials.
Especially in the drivetrain of mobility systems, lightweight components can be deployed advantageously since those machine parts are subjected to external and internal acceleration, i.e. movement of the vehicle as well as rotation of drivetrain components.
To reach a high lightweight design level, the extremely high strength and stiffness in fiber parallel direction has to be utilized while the much lower mechanical performance perpendicular to fiber direction has to be respected. This usually can be achieved better in one- or two-dimensionally loaded parts like driveshafts compared to complexly loaded components, e.g. compact mounting brackets.
In this context, driveshafts were among the first automobile components that were chosen for a industrial deployment of CFRPs in the 1980s [3]. To meet today's tightening economic requirements, major advances in the processing of composites have to be achieved [4]. Also, the development of new components has to be simplified by provision of standardized and scalable designs and composite adapted machine elements.
To address those needs, a novel design for CFRP driveshafts was developed at the Institute of Lightweight Engineering and Polymer Technology (ILK) of the Technische Universität Dresden (TUD). It is based on a profiled driveshaft body which offers the possibility of continuous manufacturing and efficient assembly processes. This generic design can easily be adapted to different applications and thus promises a significant reduction of development time.

2 The design guideline 'GWeN'

To reduce the threshold for the use of CFRPs in lightweight components, the ILK is not only developing new designs and processes, but is also building design guidelines for the industrial developer. One example with the focus on driveshafts is the 'Design guideline for shaft-hub connections (GWeN)' [5].

2.1 Regarded connection types

The work in this research project comprises three connection types, which are investigated thoroughly (see FIG. 1).

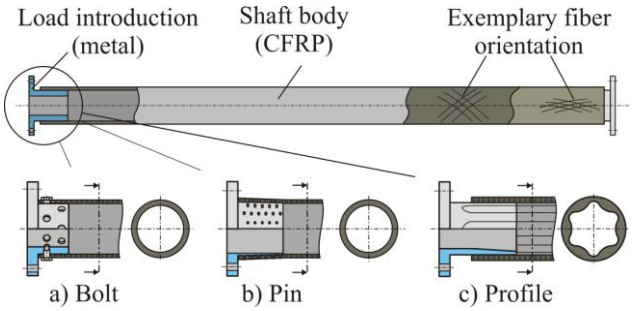

FIG. 1: Connection types regarded in the design guideline 'GWeN'

The bolted connection acts as the reference system since it is one of the classical hub-shaft-connection types for composite driveshafts. For this well established connection type, standardized design instructions already exist [6].

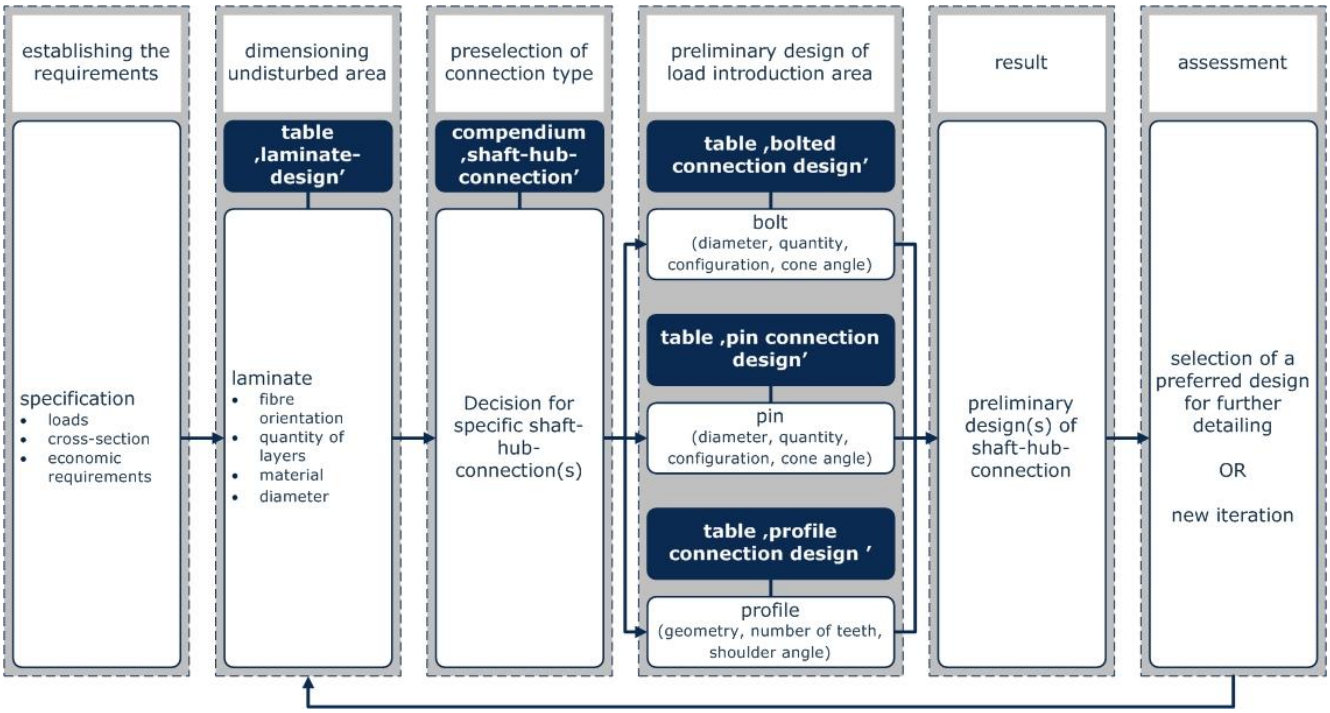

FIG. 2: Overview Chart for the Design guideline GWeN

The pin connection was first presented by the Austrian company 'Teufelberger' and promises very high load introduction capabilities. Through integrating the metallic pins into the textile perform prior to consolidating the CFRP, a mixed connection with proportions of adhesive bonding and form-fit is generated. To current date, no design instruction is known for that novel connection type.

The smoothed spline (SSP-)connection for CFRP driveshafts was developed at the ILK [7]. It offers a high load introduction capability via form fit that requires no primary assembly processes such as milling and bolting. The fiber-adapted spline joint cross section is generated during the manufacturing process. It is producible utilizing continuous manufacturing processes.

2.2 Scope of the investigations

Aim of the presented research project is the provision of easily usable design notes to allow for a preliminary design and dimensioning of new driveshaft products.

To provide a sound foundation for those design notes, material parameters are determined experimentally and parametrical simulations are conducted. The manufacture and testing of prototypes completes the investigations. Using the experimental results, simulation models are calibrated and validated. The prototype manufacturing allows for a first assessment of production effort and cost.

2.3 Overview page

The developed path to the preliminary design of a new driveshaft product is summarized in the diagrammatic plan above (FIG. 2)

Modeled on a classical development roadmap, the design guideline first needs the ancillary conditions such as available design space, mechanical and medial loads and economic requirements as input data. First, a rough laminate layup is to be taken out of a table compilation that covers many industry-relevant requirements.

In combination with an economical assessment, a preselection for the connection type can be achieved. Then the preselected connection type is preliminarily dimensioned. If the connection still satisfies the requirements, a detailed dimensioning and design is necessary. The process can also be repeated in an iterative approach, until a viable design is found.

In the following, this paper concentrates on the ILK-own profiled driveshaft concept. In previous investigations, it had shown an excellent load bearing capability while allowing for productive and efficient manufacturing and assembly processes [8].

3 Design and manufacturing of profiled driveshafts

In analogy to metallic machine parts, one way of reducing component cost for composite parts is seen in the use of standardized semi-finished products. Those can be produced in high numbers and then fitted to the final application. Following this idea, a driveshaft system concept was developed at the ILK, where different functional components such as flanges or gear wheels, universal joints or bearings can be taken out of a standardized catalogue and be assembled with a profiled shaft body to form a customized drivetrain component [9]. This concept was developed further with respect to high performance applications.

3.1 Driveshaft concept

The newly developed driveshaft concept focuses on the provision of high performance semi-finished driveshaft bodies, which are equipped with metallic end fittings for concentrated load introduction (see FIG. 1).
For highest mechanical performances, a basic geometry as depicted in FIG. 3 is chosen. It features a profiled inner laminate (I) for load introduction, supplemented by axial reinforcements (II) and enclosed by a cylindrical laminate (III) for load transmission over the span of the driveshaft.

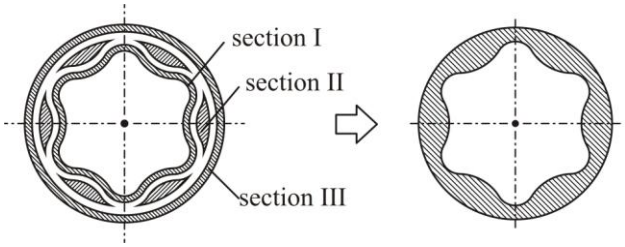

FIG. 3: Schematic buildup of profiled shafts with separated subareas (left), as monolithic part (middle), investigated sub-model (right)

In order to maintain the advantage a continuous manufacturing process, the profile is linearly extruded to constitute the shaft body. Thus, the profile geometry not only influences the load introduction capabilities, but also the mechanical performance of the shaft in the ‘undisturbed’ area. Those two features have to be matched in order to develop a viable design.

3.2 State of stress and failure phenomena

To identify the most critical regions of the cross-section, the local loading is examined and compared with experimental results (FIG. 4 and FIG. 5).

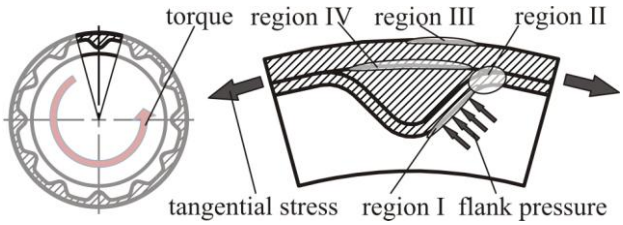

FIG. 4: Examined driveshaft section (left), local areas of interest (right)

The load is transmitted at the tooth shoulders resulting in a contact pressure (I). It induces a notch stress in the tooth root (II) as well as local tension stresses in the cylindrical areas (III). Because of the angled tooth flank, a tangential stress is induced, resembling an inner pressure load. Additionally, the introduced load has to be transferred into the outer cylindrical laminate resulting in shear stresses (IV). The comparison with first shaft specimen shows three dominant failure phenomena in the load introduction zone (compare FIG. 5).
For the first finite element studies, the effects II, III, IV and the tangential stresses are focused in the assessment of profile geometries.

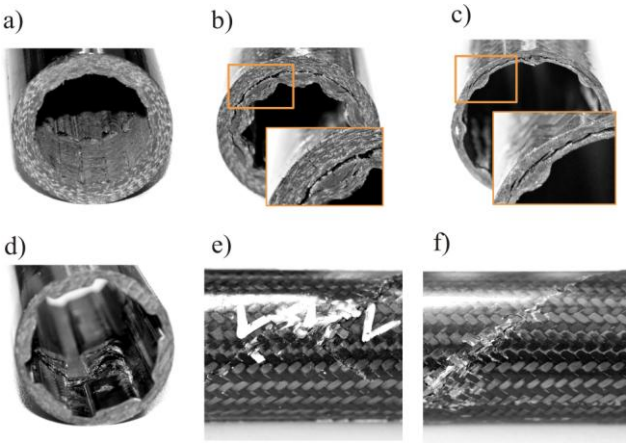

FIG. 5: Experimentally observed failure phenomena: a) tooth barring b/c) interlaminar shear d/e) shaft fracture at the end of the load introduction f) torque failure of the shaft body

3.3 Serial manufacturing concept

The basic concept of the investigated driveshaft is focused on a continuous manufacturing process. By eliminating manual process steps and utilizing highly productive performing processes such as braiding or continuous winding (FIG. 6), the part cost can be significantly reduced while enhancing reproducibility of the manufacturing results.

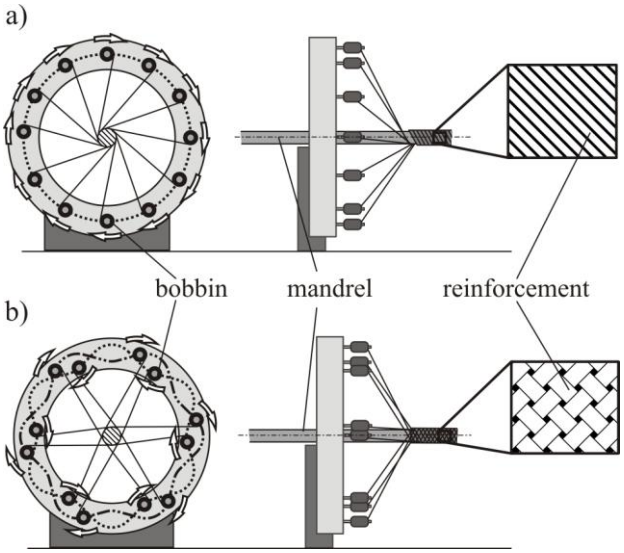

FIG. 6: Continuous fiber layup processes a) Continuous winding (unidirectional reinforcement) b) Braiding (bi-directional, textile reinforcement)

The choice of the preforming process influences the part performance, since the resulting reinforcement architectures differ in their characteristics. Unidirectional reinforcements (continuous winding) feature highest mechanical properties, due to a low level of fiber undulation. Bi-directional reinforcements obtained by braiding usually exhibit a textile binding with fiber undulation and interlocking of fibers. Compared with unidirectionally reinforced parts, they tend to perform poorer when tested in the original state, but their damage tolerance is usually higher [10, 11]. Thus, the overall performance of the developed driveshaft can be tailored to the specific application.

The general concept for serial manufacturing feasible for both preforming processes - is depicted in FIG. 7:

- Preforming of the profiled laminate on a continuously fed mandrel
- Forming of the profile
- Supply of the axial reinforcement
- Preforming of the cylindrical outer laminate
- Consolidation in a pultrusion nozzle or cutting of the preform and insertion into a RTM Tool

One of the main challenges is the reproducible forming of the profiled laminate. For this task, a preforming device was developed at the ILK and the Leichtbau-Zentrum Sachsen GmbH (compare section 5.1). With the successful testing of the continuous preforming, the elaborated serial manufacturing process is validated (compare section 5).

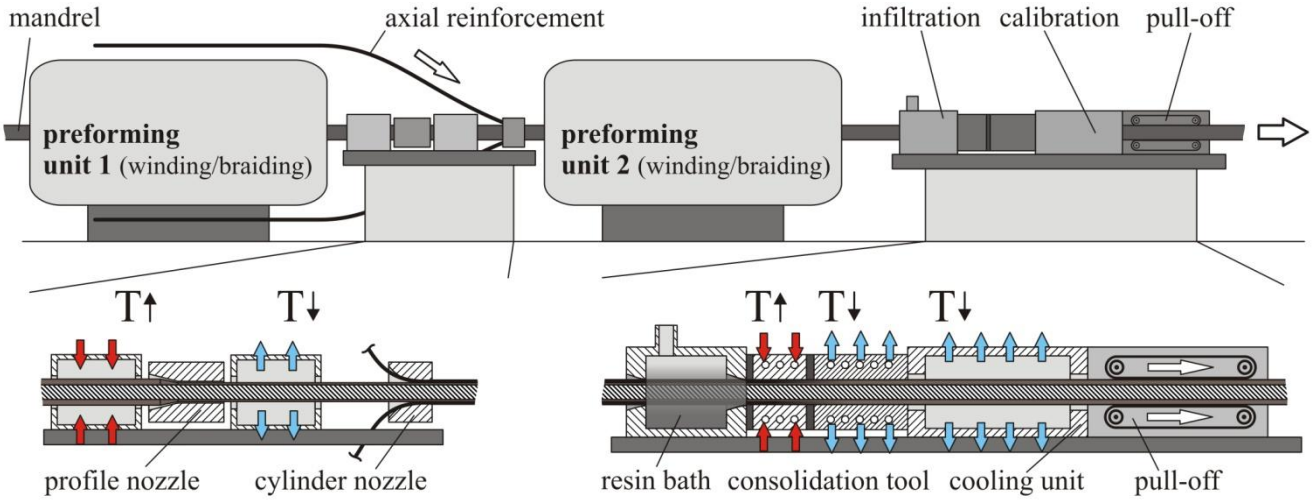

FIG. 7: Concept for a continuous manufacturing of profiled driveshafts: Overview on the production line (above), schematic representation of the profile forming (below left), schematic representation of a pultrusion array for infiltration and consolidation of the shaft laminate (below right)

4. Numerical simulations

4.1 FE-Model

The cross-section of the developed shafts exhibits filigree geometrical features. In order to model local stress effects occurring in and around the composite teeth, the element length was chosen with an average of 0,3 mm (FIG. 8).

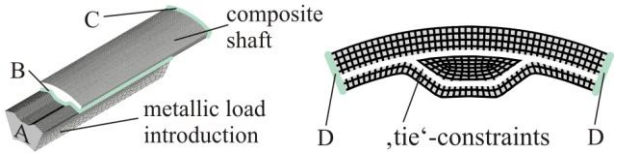

FIG. 8: Parametric FE-Model: Overview and boundary conditions (left), detailed depiction of composite shaft mesh (right)

The model buildup mirrors the actual geometrical buildup with the profiled inner section I, axial reinforcements II and a cylindrical outer section III. Between those three sections, a 'tie'-constraint is established. Furthermore, the cyclic symmetry of the shaft cross-section is utilized. An overview on the boundary conditions is given in TAB. 1. To economize parameter studies, the model is built starting with geometrical parameters. The meshing and the placement of boundary conditions are carried out automatically.

TAB. 1: Boundary conditions in the developed FE-Model

region	boundary condition	remark
A	bearing	no translation in axial direction
	force	in tangential direction (torque)
B	contact	Frictional coefficient $\mu = 0.1$
C	bearing	no translation in axial and tangential direction
D	cyclic symmetry	

4.2 Regarded failure effects

The failure prediction on unidirectional laminates in stretched areas of the simulated parts can be successfully performed using established failure criteria like HASHIN/PUCK or CUNTZE [12,13]. For geometrically complex model areas, or when textile reinforcements are utilized, the accurate prediction of laminate failure is more challenging. At the ILK, a failure prediction approach for bi-directional reinforcements by CUNTZE is used and was experimentally investigated [14]. Following this experience, the criterion 'CUNTZE BD' is used for assessment of the laminate stresses of region II and III (FIG. 4), since the tested specimen are manufactured using a braided textile reinforcement. The description of the utilized failure criterion is to be found in [15, 16] while the main formula is given with (1).

The failure mode in region IV is not covered by the utilized criteria, which only regard 'in-plane' failure. To include this failure mode, which proved to be crucial for certain profile geometries, a customized criterion was developed.

Assuming that inter fiber failure modes are matrix dominated and these modes are also causing interlaminar failures, the CUNTZE-criterion as given in (1) was reformulated to match the stress state consisting of radial tension/compression σ_3 and tangential shear stress τ_{23} (2).

$$\left(\frac{\sigma_2+|\sigma_2|}{2R_{22}^t}\right)^m+\left(\frac{\tau_{12}}{R_{12}-b_{12}\sigma_2}\right)^m+\left(\frac{-\sigma_2+|\sigma_2|}{2R_{22}^c}\right)^m=1 \qquad (1)$$

$$\left(\frac{\sigma_3+|\sigma_3|}{2R_{33}^t}\right)^m+\left(\frac{\tau_{23}}{R_{23}-b_{23}\sigma_3}\right)^m+\left(\frac{-\sigma_3+|\sigma_3|}{2R_{33}^c}\right)^m=1 \qquad (2)$$

The corresponding graphic interpretation is given in FIG. 9.

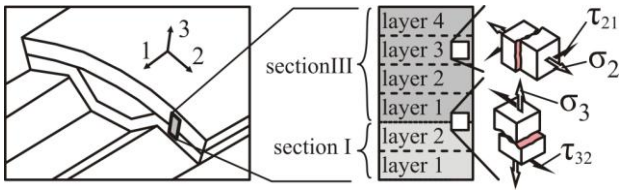

FIG. 9: Areas of interest for the failure prediction in area IV: Orientation of the in-plane intralaminar CUNTZE criterion (top right), orientation of the adapted out-of-plane interlaminar criterion (bottom right)

In the established failure criteria for fiber reinforced plastics, an interference of tension/compression and shear loading perpendicular to fiber direction is respected. Under compression, the laminate can resist a significantly higher shear stress compared to when under tension. This same effect is assumed for the shear-loaded interlaminar layer in area IV. FIG. 10 shows the corresponding failure curve and illustrates the assumed increase of the shear strength under compression between both layers.

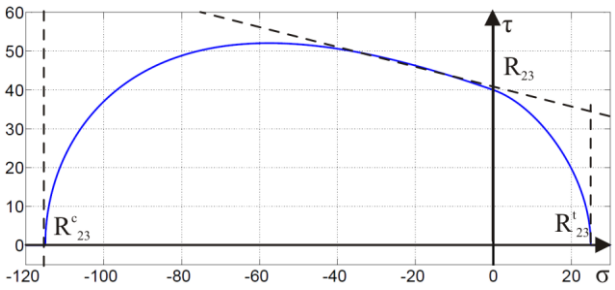

FIG. 10: Implemented failure curve for the out-of-plane interlaminar material effort.

This curve was obtained using customary data for carbon fiber reinforced epoxies available in the ILK-database (TAB. 2)

TAB. 2: Customary strength data for carbon fiber reinforced epoxy

strength identifier	value [MPa]	explication
R_{23}	40	shear strength in the 23-direction
R^t_{23}	25	tensile strength perpendicular to fiber direction
R^c_{23}	115	compressive strength perpendicular to fiber direction

4.3 Simulated profile geometries

Four profile geometries were chosen to be manufactured, tested and simulated (see FIG. 11).

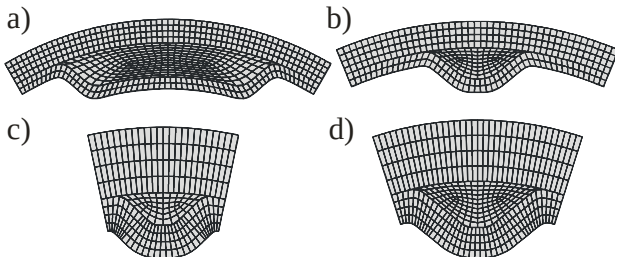

FIG. 11: Simulated shaft geometries: a) Geo1 b) Geo2 c) Geo3 d) Geo4

The geometries Geo1 & Geo2 were designed with a thin laminate (1.6 mm, layup 1), Geo3 & Geo4 with a thick laminate (4 mm, layup 2) (compare TAB. 4). All shafts possess an outer diameter of 30 mm.
The failure criteria used for the prediction of the ultimate torque capacity are assigned to the different regions of interest as depicted in TAB. 3

TAB. 3: Assignment of interpreted failure criteria to the regions of interest

region	underlying criterion	analyzed mode	denomination
II	CUNTZE BD	fiber fracture	CUNTZE B
III	CUNTZE BD	resulting effort	CUNTZE A
IV	CUNTZE UD	-	Shear Criterion

5. Experimental investigations

To assess the load bearing capacity of the developed driveshafts, a variety of test specimen was manufactured and tested. The geometries were chosen with a wide modification of shape, in order to enable a comparison with the numerical models on different interpolation points.

5.1 Prototypic manufacturing

For the prototypic manufacturing, commercially available braided sleeves are utilized. To confirm the continuous manufacturing principle, the preforming has to be performed under constant feed of the mandrel. This is achieved in a prototypic installation shown in FIG. 12.

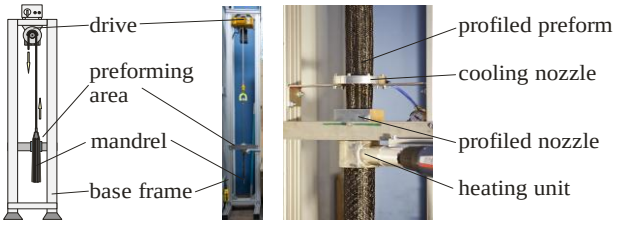

FIG. 12: Prototypic test stand for investigations on profile forming parameters: Schematic representation (left), realized device (right)

With the use of a binder material (XB3366, HUNTSMAN chemicals), the preform is held in shape. Subsequently, the axial reinforcements are placed on the mandrel and it is covered with the braided sleeves forming the cylindrical laminate (Layup I, TAB. 4). The finished preform is then inserted into a RTM-Tooling and infiltrated with the Epoxy resin ‘Araldite LY556 / Aradur HY917’ (HUNTSMAN Chemicals). The manufactured shaft body is then cut into four pieces with a length of 170 mm each.

TAB. 4: Laminate layup overview

layup	layers	orientation	thickness
1	1-2	+- 45°	0,53 mm
	3	0°	-
	4-7	+- 45°	1,06 mm
2	1-2	+- 45°	1,33 mm
	3	0°	-
	4-7	+- 45°	2,66 mm

5.2 Mechanical testing

The manufactured specimens are subjected to torque loading, using a tension-torsion testing machine ‘Zwick/Roell Z250’ with the ultimate torque capacity of 2000 Nm. The test is performed under compensation of axial loads with an application of torque using a twist speed 5°/min (quasi-static).
To get a first indication on the dynamic behavior, the load is applied in load steps (see FIG. 13). To determine a suitable start value ‘A’, one specimen for each geometry is tested for failure. ‘A’ is then chosen with half the failure load. If no failure occurs, the load level is increased successively by 50 Nm until a failure is detected.

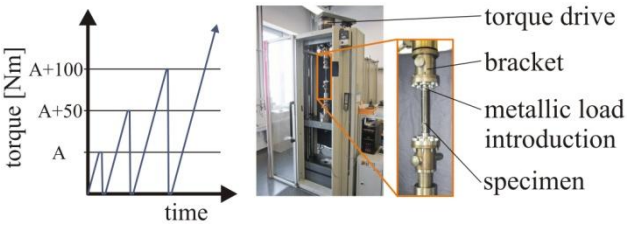

FIG. 13: Load step configuration (left), torque test set up (right)

5.3 Results

The following figure shows the achieved failure load levels with a reference to the shaft cross-section (FIG. 13). The very small deviations in failure loads indicate a reproducible process.

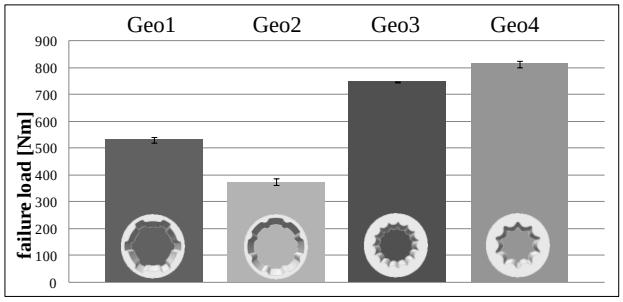

FIG. 14: Ultimate torque capacity of driveshaft test specimen wit different geometries of the cross section

The following figures show the prediction accuracy of the applied failure criteria. In the background columns (light grey), the experimentally determined failure load is given. In the front columns (dark grey), the predicted load bearing capacity of the shaft according to the three different criteria is shown. The white numbers give the material effort for each criterion with a value of '1' implying failure. A white frame highlights the predominant failure phenomenology as observed in the experiment.

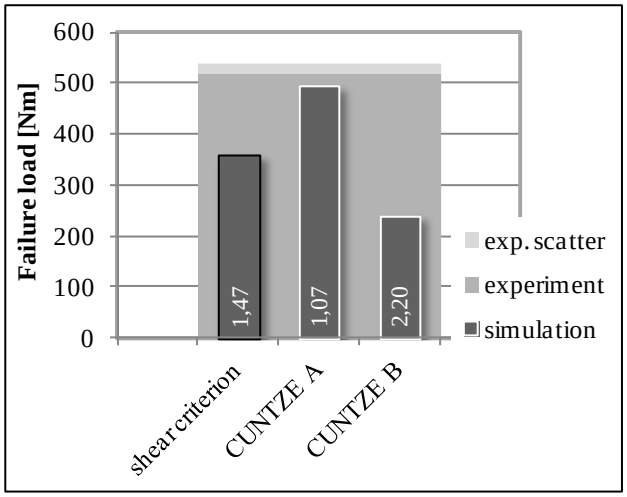

FIG. 15: Experimental failure load for shaft geometry Geo1 (light grey, background) compared with predicted failure loads according to the different failure criteria (dark grey)

For shaft geometry Geo1, a high level of material utilization was reached. All predicted load bearing capacities were exceeded by the experimental values (FIG. 15). The failure phenomenology resembled the pictures d/e/f in FIG. 5.

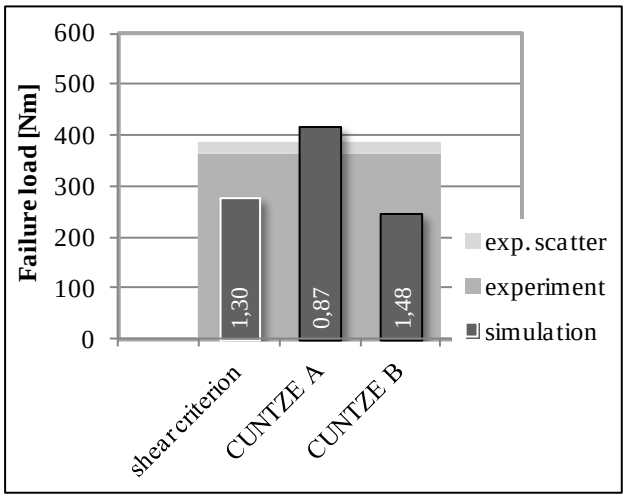

FIG. 16: Experimental failure load for shaft geometry Geo2 (light grey, background) compared with predicted failure loads according to the different failure criteria (dark grey)

Shafts with geometry Geo1 feature eight less pronounced teeth. Those fail according to phenomenology b/c in FIG. 5 due to interlaminar shear in region IV (FIG. 4). The material effort in region II and III is also high with values of 1,48 and 0,87 (FIG. 16).

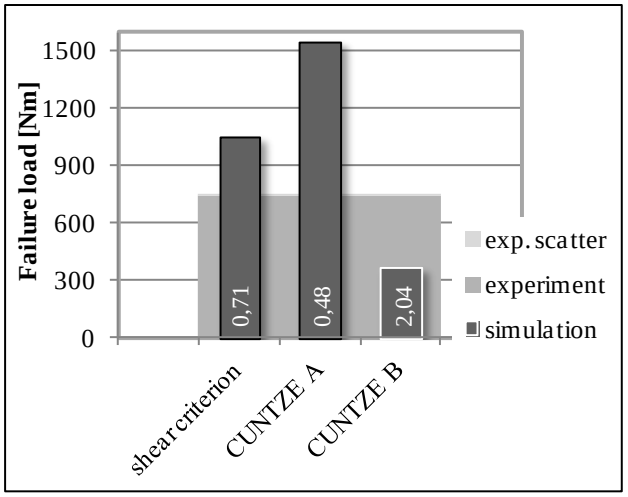

FIG. 17: Experimental failure load for shaft geometry Geo3 (light grey, background) compared with predicted failure loads according to the different failure criteria (dark grey)

For the shaft geometries with the thick walled laminate, the material effort in the region IV drops to a level of approximately 50% (FIG. 17, FIG. 18). Accordingly, the shafts featuring Geo3 fail with bared teeth (picture 'a' in FIG. 5), the shafts featuring

Geo4 fail due to shear. This behavior agrees well with the calculated material efforts.

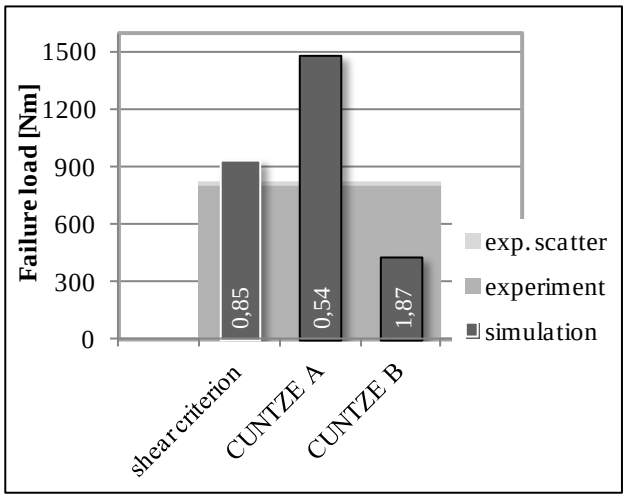

FIG. 18: Experimental failure load for shaft geometry Geo4 (light grey, background) compared with predicted failure loads according to the different failure criteria (dark grey)

When comparing the experimental results with the simulation results, the following observations can be made:

- The newly developed shear criterion predicts the failure with an accuracy of -32% and +29% or better
- For the thin walled geometries, the failure prediction in region III by the CUNTZE BD criterion exhibited an accuracy of +7% and -13%
- The fiber failure criterion in region II is conservative with a factor of 2,2 or 2,04 respectively when fiber fracture in the teeth root is a predominant failure mode.

The deviations in the results could be attributed to the input material data and the complex stress state in the examined regions of interest. A repetition of simulations with especially determined material data is advised.

6. Conclusions

In this paper, a novel approach to design, dimensioning and manufacturing for high performance composite driveshafts is presented. After introducing the design guideline GWeN for the efficient development of composite driveshaft products, the investigations concerning a shaft-hub connection with a profiled shaft cross-section are presented.
Besides mechanical performance, this connection type is designed for a highly automatable, continuous manufacturing and an efficient assembly process. The shape of the cross section is dominant not only for load introduction but also for the global mechanical performance of the shaft. Therefore, a parametrical, highly detailed FE-Model was created and used for the simulation of the mechanical load bearing behavior. To take into account the specific failure phenomenology, a novel failure criterion for interlaminar shear was developed on the basis of the well established CUNTZE failure criterion.
To assess the load bearing capacity of the novel shaft-hub-connection prototypic shafts have been manufactured and tested. The prototypic manufacturing procedure was using a continuous preforming process, thus validating the developed serial manufacturing process. High failure loads with very low scatter indicate an excellent reproducibility of the elaborated manufacturing concept.
The comparison of experimental test results with the performed simulations, utilizing the especially developed interlaminar Shear Criterion, show good agreement.

7. Acknowledgements

The development of the design guideline ‘GWeN’ and the affiliated numerical and experimental investigations has been performed in the project ‘Ultraleichte Antriebswelle’ funded by the Arbeitsgemeinschaft industrieller Forschungsvereinigungen (AiF) and the Forschungsvereinigung Verbrennungskraftmaschinen e.V. (FVV). The work on a serial manufacturing process has been performed inter alia in the research project ‘MOLEW’, funded by the European Fund for Regional Development (EFRE) and the Fraunhofer IWS Dresden in the Dresdner Innovationszentrum für Energieeffizienz (DIZE^{eff}). The authors thank all involved entities for the financial and strategic support.

References

[1] Darecki M. et al. “Flightpath 2050 – Europe’s Vision for Aviation”. *Publications Office of the European Union*, 2011

[2] Pötscher F., Read B. Schneider J. „Modalities for reaching the 2020 target to reduce CO2 emissions from new passenger cars” *Publications Office of the European Union*, 2013

[3] H. Haldenwanger “*Development of plastics parts for the racing and standard versions of the Audi-Quattro*”. Society of Automotive Engineers, 1982.

[4] R. Lässig, M. Eisenhut, A. Mathias, R. T. Schulte, F. Peters, T. Kühmann, T. Waldmann and W. Begemann: "*Serienproduktion von hochfesten Faserverbundbauteilen"* VDMA Verlag, 2012.

[5] W. Hufenbach, F. Lenz, S. Spitzer, O. Renner "Welle-Nabe-Verbindungen für Leichtbau-Antriebswellen in Faserverbund-Metall-Mischbauweise" *VDI-Tagung*, Nürtingen, VDI-Berichte Nr. 2176, 2012.

[6] VDI-Society Materials Engineering "*VDI 2014/3 - Development of fibre-reinforced plastics components-Analysis"*. German Association of Engineers, 2006.

[7] W. Hufenbach, O. Helms and J. Werner "Welle-Nabe-Verbindungen für hoch beanspruchte Antriebskomponenten in Faserverbund-Leichtbauweise" *VDI-Tagung*, Wiesloch, VDI-Berichte Nr. 2004, 2007

[8] W. Hufenbach, F. Lenz "Methodical design of load adapted hybrid structures for aerospace applications" Oral presentation. *EUCOMAS*, Hamburg, 2012.

[9] W. Hufenbach, O. Helms, J. Werner "Hohlwelle aus Faserverbundwerkstoff und darauf zu befestigende Funktionselemente" Patent Application, DE 10 2007 051 517 A1, 2007

[10] J. K. Kim, M. L. Sham "Impact and delamination failure of woven-fabric composites". *Composites Science and Technology*; Vol. 60; pp. 745-761, 2000.

[11] J. K. Kim "Methods for Improving Impact Damage Resistance of CFRP". *Key Engineering Materials*; pp. 141-143; 149-168, 1998.

[12] M. J. Hinton, a. S. Kaddour, P. D. Soden "*Failure Criteria in Fibre Reinforced Polymer Composites: The World-Wide Failure Exercise"*. Elsevier Ltd. 2004.

[13] R. G. Cuntze "The Failure Mode Concept- A new comprehensive 3d-strength analysis concept for any brittle and ductile behaving material". *Proceedings of the European Conference on Spacecraft Structures, Materials and Mechanical testing*, Braunschweig,, pp 269-287, November 1998.

[14] A. Ulbricht *"Zur Gestaltung und Dimensionierung von zylindrischen Leichtbaustrukturen in Faserkunststoffverbund-Metall-Mischbauweise"*. Dissertation, Technische Universität Dresden, 2011.

[15] R. G. Cuntze, A. Freund "The predictive capability of failure mode concept –based strength criteria for multidirectional laminates". *Composite Science and Technology*, Vol. 64, Issues 3-4, pp 343-377, 2004.

[16] R. G. Cuntze "Failure conditions for isotropic materials,uni-directional composites, woven fabrics – their visualization and links ". *Proceedings of the Conference on Damage in Composite Materials*, Stuttgart, 2006.

IMPREGNATION PROCESS FOR FIBER HYBRID BRAIDED THERMOPLASTIC COMPOSITES

T. Motochika[1*], K. Nakazawa[2], A. Ohtani[1], A. Nakai[1]
[1] Faculty of Engineering, Gifu University, Gifu, Japan
[2] Advanced Fibro-Science, Kyoto Institute of Technology, Kyoto, Japan
T. Motochika (t.motochika.1987@gmail.com)

Keywords: *FRTP, Fiber hybrid, Braided composite, Pultrusion*

1 Introduction

Hybrid composite have been researched by many researchers because hybrid fiber or resin gives composite great mechanical performance which composite made from sole fiber or resin does not achieve. Hybrid composites are expected to be highly-functional properties because of eliminating weakness and developing merit each other. Most popular hybrid composite is hybrid fiber composite and two or more different reinforcing fibers such as glass fiber, carbon fiber and aramid fiber are used in one composite[1].

In this study, braiding structure was employed as reinforcements to achieve hybrid fiber structure. In braided fabrics, the fiber bundle called middle end yarn (MEY) can be inserted between braiding fibers in longitudinal direction, so that the excellent mechanical properties were expected. In addition, the braided fabrics by using various kinds of braiding fiber and MEY with different properties can be fabricated. Therefore, concept of hybrid composite can be easily applied by using braiding technology and the mechanical properties of the braided composite can be designed according to the requirements. The concept of fiber hybrid composite was expansively applied to FRTP[2].

The purpose of this study is to clarify the impregnation process of hybrid fiber braided FRTP and relationship between impregnation property and mechanical property. In order to examine the impregnation process, cross-sectional observation of moldings with different molding time and braiding structure was performed.After that, impregnation process of fiber hybrid FRTP for pultrusion was investigated by stopping pultrusion molding in midstream and effect caused by pultrusion speed to impregnation state.

2 Materials and molding method

2.1 Intermediate materials

To clarify the process of impregnation for fiber hybrid FRTP, carbon fiber (T700-50C-12000 (sizing content : 1.1wt%), T700-60E-12000 (sizing content: 0.2wt%), 800tex, TORAY) and aramid fiber (Kevlar29-12000 660tex, TORAY Dupont) were used as the reinforcement while the PA66 resin fiber (L-235T35B PA66235dtex, melting temperature: 265 ℃) was used as the matrix resin. Commingled yarns made from these materials are listhed in Table1. “Com-” indicates “Commingled yarn of”, CH and CL indicates carbon fiber with high or low sizing content. Vfi was defined as the Vf of reinforcing fiber at intermediate material. Dispersion ratio was defined as the ratio of dispersion between reinforcing fiber and resin fiber. If dispersion ratio was increased, impregnation distance was decreased.

Table 1 Commingled yarns.

Sample name	Reinforcing fiber	Vfi(%)	Dispersionratio(%)	Contact angle (deg)
Com-CH	Carbon fiber (1.1wt%)	48	58.6	33
Com-CL	Carbon fiber (0.2wt%)	48	79.6	8
Com-A	Aramid fiber	49	68.7	10

2.2 Fabric

The structure of braided fabric for heat compressing was shown in Figure 1. Carbon fiber or aramid fiber and PA66 were commingled and it was used as the braided yarns (BYs) and MEYs. Tubular braided fabric was fabricated with 16BYs and 8 MEYs.

In this study, 5 types of braided fabric were used as specimen for molding. These braided fabrics are listed in Table 2. The left side of sample name means the reinforcement fiber used as braiding yarn andthe right side of sample name means the reinforcement fiber used as MEY.

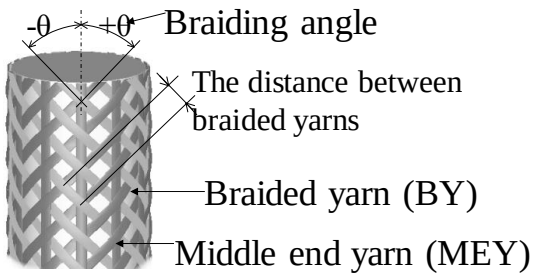

Figure 1 Structure of braided fabric.

Table 2 5 types of braided fabric.

Sample name	A/A	CH/CH	CL/CL	A/CH	A/CL
Braided yarn	Com-A	Com-CH	Com-CL	Com-A	Com-A
Middle end yarn	Com-A	Com-CH	Com-CL	Com-CH	Com-CL

3 Molding method and condition

3.1 Heat compressing

In order to investigate the impregnation state of fiber hybrid FRTP and sole FRTP, braided composite was fabricated by compression machine as shown in Figure 2. Braided fabric was inserted into molding die and was molded. Molding pressure and temperature were kept as 0.1MPa and 290 degree, the molding time was changed as 1, 3, 5, 10, 15min. Finally, braided composite plate (20mm in width, 200mm in length) was molded and the cross-sectional observation was carried out.

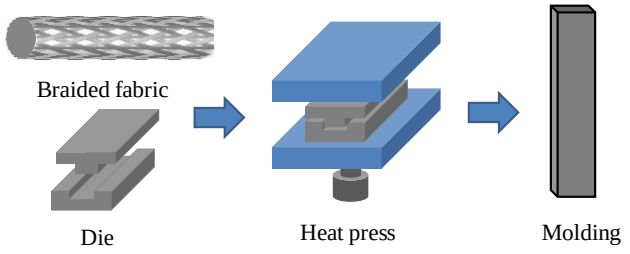

Figure 2 Heat compressing.

3.2 Pultrusion

The pultrusion line is shown in Figure 3. Braided fabrics were pulled into the pultrusion die having a cylindrical hole. During the passage into the die, the resin fiber of the braided fabric melted and impregnated into reinforcing fiber. A preheating die and a molding die were prepared for the forming of the pipe. The braided fabrics were pre-heated in the preheating die up to near melting temperature (160 ℃) of the resin fiber for easier impregnation. The molding die had the cylindrical hole with 18 mm diameter and diameter of the mandrel was 15mm, so the cylindrical tube with 1.5mm thickness was obtained by this pultrusion system.

The molding die is shown in Figure 4. The length of the molding die was 1500 mm, which was separated into 8 heating zones. The temperature at each sections of the molding die was set at 290, 290, 290, 290, 290, 285, 280, 275℃ from the entrance side, respectively. The mandrel had also a heater and set at 230℃ during pultrusion. The pipe was pulled out continuously by pulling system.

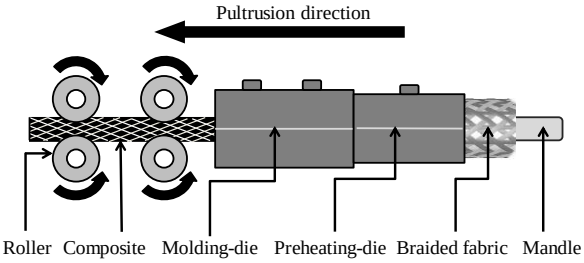

Figure 3 Pultrusion system.

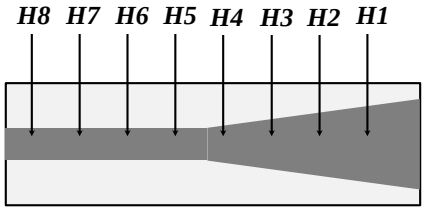

Figure 4 Positions of heaters.

3.3 Stopping pultrusion in midstream

In order to investigate the impregnation process during molding, pultrusion molding was interrupted. Then the sample inside of the molding die was taken out and cross-sectional observation of the composite cut in each position corresponding to (a) to (e) in Figure 5 was carried out by using optical microscopy. In this stopping pultrusion in mid-stream, braided fabrics of A/A, A/CL and CL/CL were used as specimen.

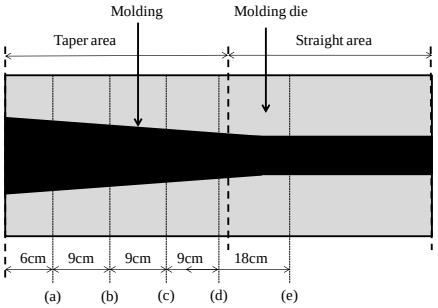

Figure 5 The points measuring impregnation ratio

4 Experiments

4.1 Dispersion ratio

In order to quantitatively evaluate the dispersion state of fibers in intermediate material, dispersion ratio was defined. The intermediate material was inserted into heat-shrinkable tube and the tube was deflated by heating. Then, the tube was formed into cylindrical shape and fibers were densely packed. The tube was embedded in a resin, and then cross-sectional observation was performed.

Figure 6 shows the definition of dispersion ratio. First, straight lines were drawn on the parabola with each 30 degree on the cross-sectional photograph. There was a continuous reinforcing fiber and resin fiber along the diameter line on the cross-sectional photograph of fiber bundle. The length of reinforcing fiber and resin fiber along the diameter line were measured. Dispersion ratio was expressed by Eq.(1).The value that average distance of first fiber-assembly to second fiber-assembly divided by total distance of both fibers was calculated. Each dispersion ratio was defined by subtracting the value from 1. As average distance of fiber area are becoming small, dispersion ratio comes close to 100%, and the minimum value is 50%.

$$\text{Dispersion ratio } (\%) = 1 - \left(\frac{\sum_{i=1}^{n} a_i \text{ or } b_i}{n} \cdot \frac{1}{\sum_{i=1}^{n} a_i, b_i} \right) \cdot 100 \quad \textbf{(1)}$$

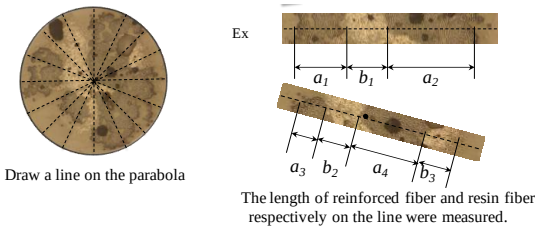

Figure 6 Definition of dispersion ratio.

4.2 Cross-sectional observation

The cross section of each molding was observed with the optical microscope. For the observation on cross section, the samples were emery grinded (#100~#2,000) and buffed (alumina particle, average particle size: 100 nm) after they were embedded in epoxy resin. After cross-sectional observation, un-impregnation ratio of each specimen was calculated. The definition of un-impregnation ratio is shown in Figure 7. Un-impregnation ratio was defined as the area of un-impregnation area divided by the area of a fiber bundle.

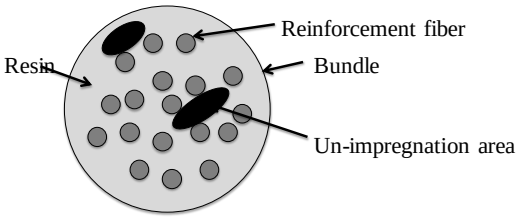

$$\text{Un-impregnation ratio} = \frac{\text{The area of un-impregnation area}}{\text{The area of bundle}}$$

Figure 7 Definition of un-impregnation ratio.

4.3 3-point bending test

The three-point bending test was conducted to estimate the mechanical properties. In this test, INSTRON type-4206 was used as the universal testing machine. Conditions of the experiment were as indicated below: span length was 80mm, specimen length was 110mm, and testing speed was 3mm/min.

5 Results

5.1 Investigation of intermediate material

In order to investigate the intermediate material, dispersion ratio and contact angle was measured as shown in Table 3. Dispersion ratio of Com-CL was the highest, that of Com-CH was the lowest. Contact angle of Com-CL was the lowest, that of Com-CH was the highest. According to these results, it was considered that impregnation property of Com-CL was best and Com-CH was poorest because of those impregnation distance and wettability.

Table 3 Dispersion ratio and contact angle

Specimen	Reinforcement fiber	Dispersion ratio (%)	Contact angle (deg)
Com-CH	CF (1.1wt%)	58.6	33
Com-CL	CF(0.2wt%)	79.6	8
Com-A	AF	68.7	10

5.2 Impregnation state for heat compressing

Cross-sections of moldings consisted from sole material molded by each condition (molding time: 1min, 15min) are shown in Figure 8 to Figure 10. Cross-sections of consisted from hybrid material molded by each condition (molding time:1min, 15min) are shown in Figure 11and Figure 12. According to Figure 8 to Figure 12, it was clarified that un-impregnation area and the area of resin-rich were decreased with increasing of molding time.

Relationship between un-impregnation ratio of sole material (CH/CH, CL/CL, A/A) is shown in

Figure13. Relationship between un-impregnation ratio of hybrid material (A/CH, A/CL) is shown in Figure 14 and Figure 15.

According to Figure 13, each un-impregnation ratio of CF with 1.1wt% of sizing content at all time was higher than that of CF with 0.2wt% of sizing content. It is because that Com-CH had low dispersion ratio and poor wetting ability because of the high sizing content

According to Figure 14, un-impregnation ratio of CH in fiber hybrid structure was decreased compared to that of CH in sole structure. The quantity of contacted resin of Com-AF around CF was increased in the case of Fiber hybrid structure of AF/CF (1.1wt %)

According to Figure 15, in the case of fiber hybrid braided fabric which has MEY with CF of 0.2wt% sizing content, the un-impregnation ratio of MEY was increased at all molding time. The thermal conductivity of CF(80~800(W/mK)) was higher than AF (2~4(W/mK)), so that MEY of CF had longer essential molding time than BY of AF . Here, essential molding time was defined as the molding time over melting temperature. The time to melting temperature of AF was longer than that of CF because of low thermal conductivity of AF.

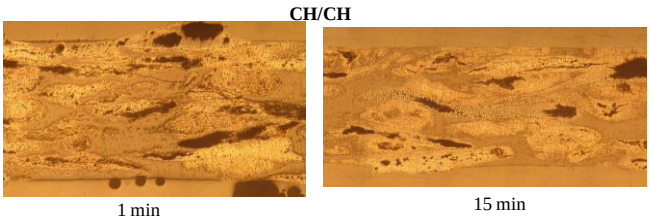

Figure 8 Cross-section of CH/CH (sole).

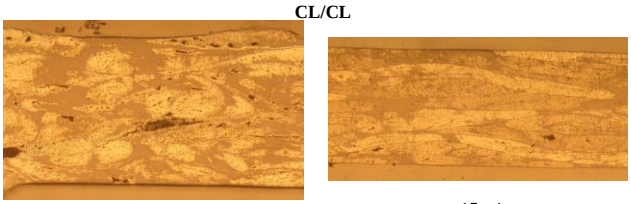

Figure 9 Cross-section of CL/CL (sole).

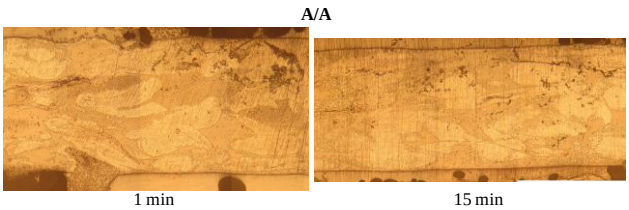

Figure 10 Cross-section of A/A (sole).

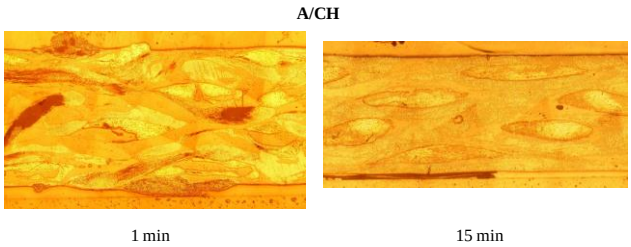

Figure 11 Cross-section of A/CH (hybrid).

Figure 12 Cross-section of A/CL (hybrid).

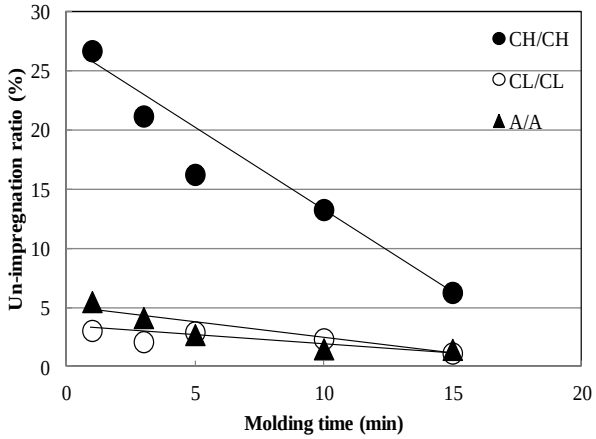

Figure 13 Impregnation process of sole composite (CH/CH, CL/CL, A/A).

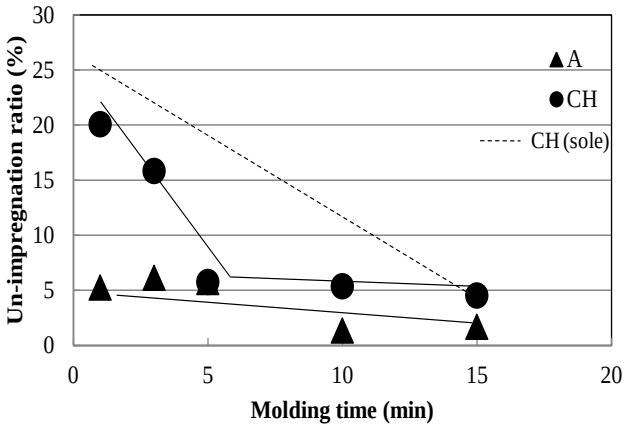

Figure 14 Impregnation process of hybrid composite (A/CH).

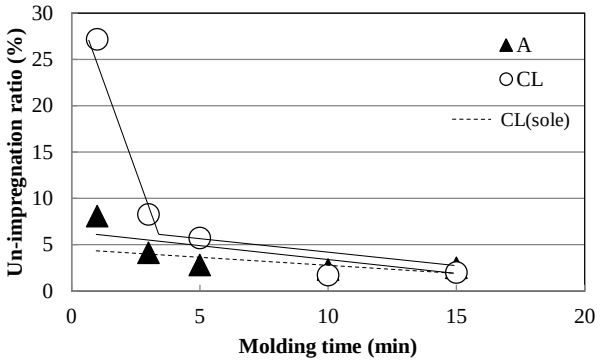

Figure 15 Impregnation process of hybrid composite (A/CL).

5.3 3-point-bending test

Specimens for 3-point-bending test were same as press molding and its molding was 15min. The result of three-point bending test was shown in Table 4. According to Table 4, comparing CH/CH and CL/CL, bending modulus and strength of CL/CL were twice higher than that of CH/CH and comparing A/CH and A/CL, bending modulus and strength of A/CL were higher than that of A/CH. The cause of these results was difference of un-impregnation ratio. It was clarified that bending modulus and strength were increased with decreasing un-impregnation ratio.

Relationship between bending modulus or strength and un-impregnation ratio was shown in Figure 16 and Figure 17. These relationships were made by CH/CH and CL/CL. According to Figure 16 and Figure 17, it was clarified that bending modulus and strength were increased with decreasing of un-impregnation ratio. This result suggested that it was important making design to decrease un-impregnation ratio.

Table 4 Result of 3-point-bending test.

Specimen	AA	CHCH	CLCL	ACH	ACL
Bending modulus (GPa)	14.7	20.2	41.2	24.6	28.4
Bending strength (MPa)	25.2	242	499	299	368
Un-impregnation ratio (%)	1.47	6.28	1.16	1.68 (BY)	2.41 (BY)
				4.52 (MEY)	2.01 (MEY)

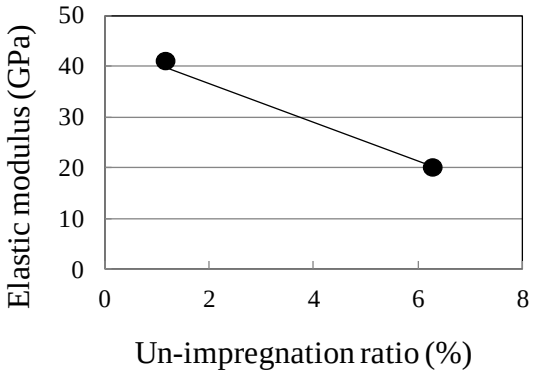

Figure 16 Relationship between elastic modulus and un-impregnation ratio.

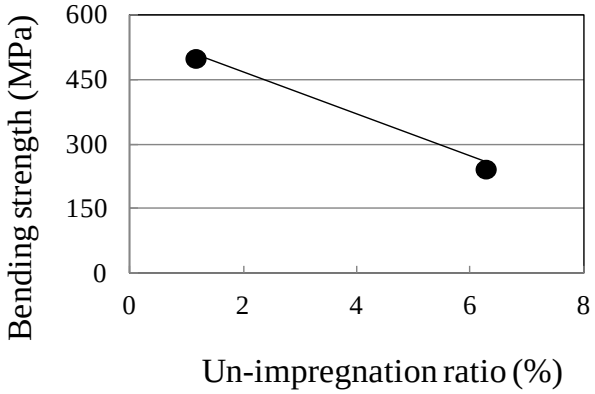

Figure 17 Relationship between bending strength and un-impregnation ratio.

5.4 Stopping pultrusion in midstream

Cross-sections of A/A, CL/CL and A/CL made by molding method of stopping pultrusion in midstream were shown in Figure 18 to Figure 20. In these pictures, width, void and un-impregnation area were decreased in tapa area of (a) to (d), but cross-section of near tapa end (d) and straight area of (e) were similar. According to this result, it was clarified that impregnation were performed only tapa area and not mostly performed in straight area.

To calculate essential molding time, temperature history was measured and shown in Figure 21. Essential molding time was defined as product set both of the time in which material was in taper zone of the molding die and the time in which material temperature was over melting temperature. Essential molding time can be calculated by temperature history and pultrusion speed. According to Figure 21, it was clarified that essential molding time was 9 min in this pultrusion design.

Relationships between un-impregnation ratio and essential molding time were shown in Figure 22 to Figure 24. In these figure, dot line show end of

molding die. In figure 22 to figure 24, first, impregnation did not start before 0 min of essential molding time because resin did not melt in this time. Second, it was clarified that un-impregnation ratio was decreased until tapa end same as cross-sections of A/A, CL/CL and A/CL.

In Figure 24, in the case of fiber hybrid braided fabric which has MEY CL, the un-impregnation ratio of MEY was increased at all molding time. This phenomenon was caused by same reason as A/CL made by heat compression in 5.2.

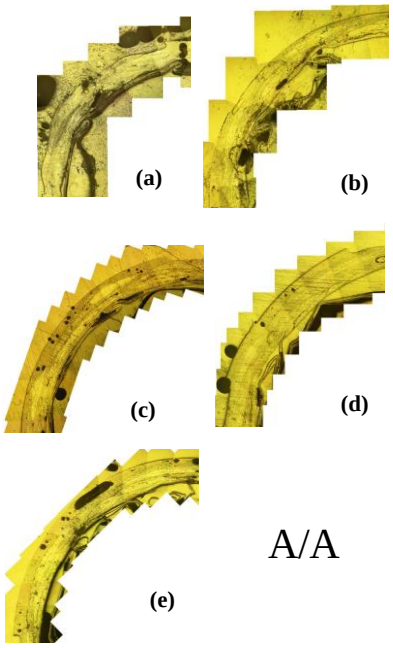

Figure 18 Impregnation process of A/A.

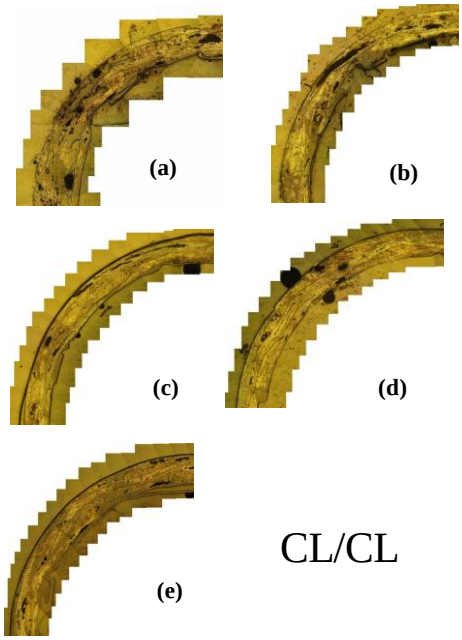

Figure 19 Impregnation process of CL/CL.

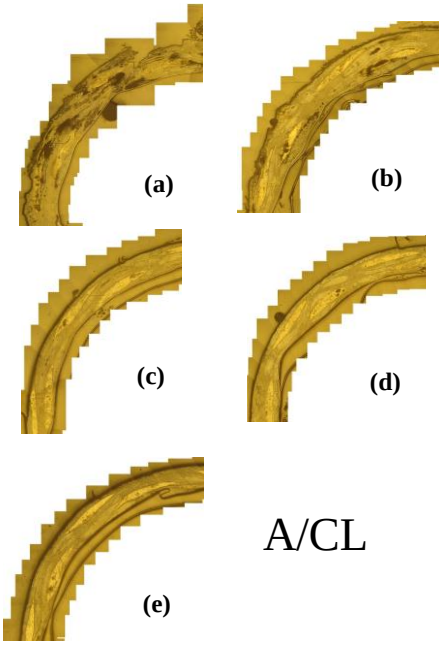

Figure 20 Impregnation process of A/CL.

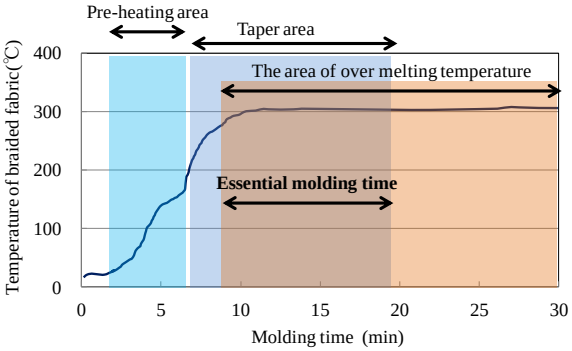

Figure 21 Temperature history of pultrusion.

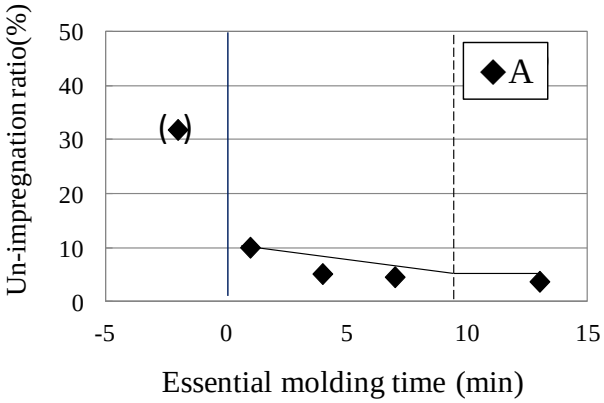

Figure 22 Relationship between un-impregnation ratio and essential molding time of A/A.

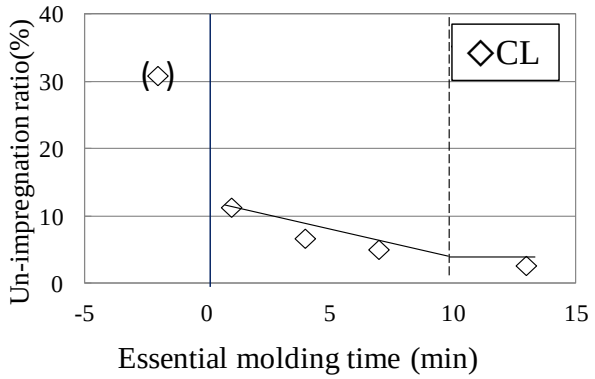

Figure 23 Relationship between un-impregnation ratio and essential molding time of CL/CL.

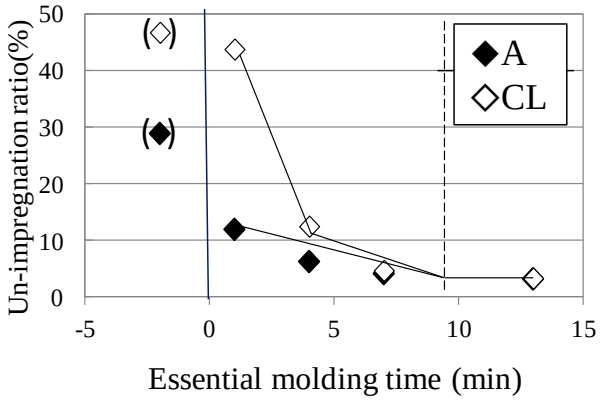

Figure 24 Relationship between un-impregnation ratio and essential molding time of A/CL.

5.5 Difference of impregnation process by heat compressing and pultrusion.

Differences of impregnation process by heat compressing and pultrusion were shown in Figure 25 and Figure 26. Difference of aramid fiber was shown in Figure 25 and difference of cabon fiber was shown in Figure 26.

In Figure 25, the curve pultrusion was in upper side comparing to the curve of heat compressing. It is considered that the reason of this gap between two curves was caused by difference of molding pressure.

In Figure 26, it is considered that the curve of pultrusion can be shifted to left by more pre-heating and the difference of convergent point was caused by molding pressure from difference molding method.

According to these result, this pultrusion system must be improved by adding longer pre-heater for longer pre-heating time and making some system for adding more pressure to braided fabric. If these system developed these system, molding which has same quality as made by heat compressing will be able to molded continuously.

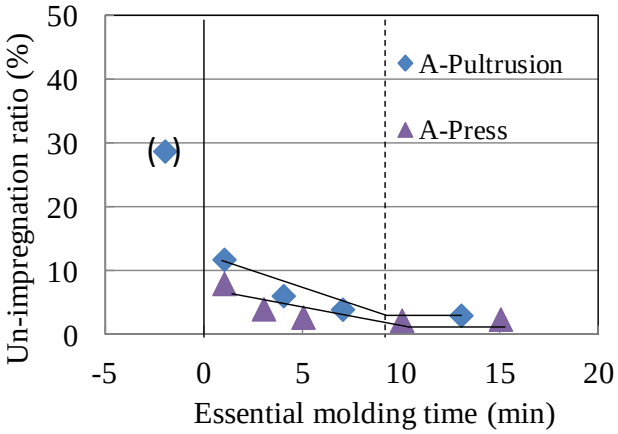

Figure 25 Difference of relationship between un-impregnation ratio and essential molding time for aramid fiber.

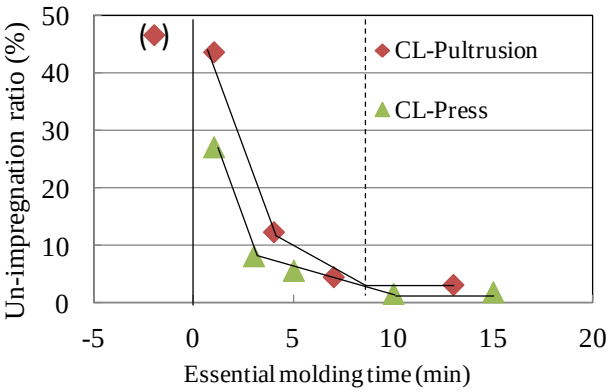

Figure 26 Difference of relationship between un-impregnation ratio and essential molding time for carbon fiber.

5.6 Effect of pultrusion speed to impregnation state of molding

In this section, to investigate effect of pultrusion speed to molding condition, pultrusion for A/CL was performed with several pultrusion speed (30, 50, 100, 150 mm/min). Molding condition was same as 3.2. Cross-sections of each speed was shown in Figure 27 to Figure 30 in order of pultrusion speed of slowness. In Figure 29 and Figure 30, pipe outer diameter s were not constant because cooling at exit of molding die was not enough. In addition, it was clarified that one layer was broken because of increasing of pultrusion friction in these Figures.

Relationship between un-impregnation ratio and pultrusion speed was shown in Figure 31. According to Figure 31, it was clarified that un-impregnation

ratio was increased with increasing of pultrusion speed. It was because that essential molding time was decreased because of decreasing of staying time in molding die if pultrusion speed was increased.

Responding to these result, it was considered that extending molding die and decreasing of pultrusion friction would be beneficial for improving of pultrusion speed.

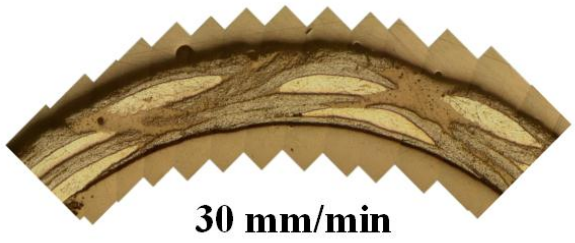

Figure 27 Cross-section of 30 mm/min.

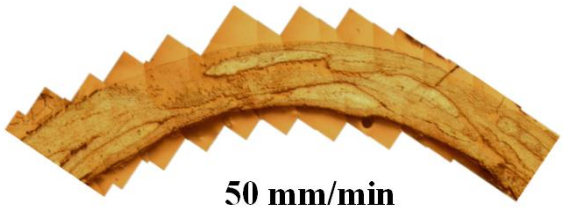

Figure 28 Cross-section of 50 mm/min.

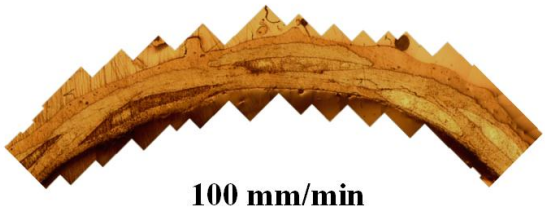

Figure 29 Cross-section of 100 mm/min.

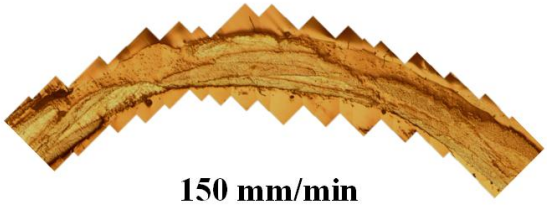

Figure 30 Cross-section of 150 mm/min.

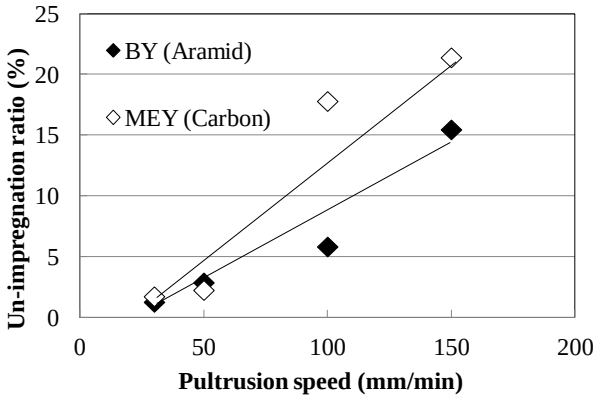

Figure 31 Relationship between un-impregnationratio and pultrusion speed

6 Conclusions

By investigation of intermediate material, the wettability of CF with lower sizing content of 0.2wt % was better than that of CF with higher sizing content of 1.1wt %.

By comparing cross-sectional observation of sole or hybrid FRTP with various molding times, it was clarified that impregnation process in same fiber bundle was changed according to the combination of AF and CF. It is considered that these results can be applied to various design of molding FRTP like pultrusion.

By investigating impregnation process of pultrusion by stopping pultrusion molding in midstream, it was clarified that impregnation was performed in only tapa area in molding die and aramid fiber filled the role of insulator to carbon fiber same as heat-compress molding.

By investigate relationship between molding state and pultrusion speed, it was clarified that molding state was made worth with increasing pultrusion speed because of decreasing essential molding time and increasing pultrusion friction.

7 Reference

[1] Toshihiro Motochika, Daisuke Hatano, Asami Nakai, Akio Otani. Pultrusion of Fiber Tubular Braided Thermoplastic Composites. B-10, 56th FRP CON-EX2011 (2011)

[2] Toshihiro Motochika, Daisuke Hatano, Asami Nakai, akio Otani. Pultrusion of Fiber Tubular Braided Thermoplastic Composites. 1134, JSCM2012/JCOM-41 (2012)